Check for updates

Synthesis, crystal structure and photoluminescence studies of [Eu(dbm)₃(impy)] and its polymer-based hybrid film†

Najmul Hasan and Khalid Iftikhar (ID)*

An eight-coordinate Eu(III) complex with 1,3-dibenzoylmethane (Hdbm) and 2-(1*H*-imidazol-2-yl)pyridine (impy), [Eu(dbm)₃(impy)], was synthesized and characterized *via* elemental analysis, FTIR spectroscopy, ESI-MS⁺ studies and thermal analysis (TGA/DTA). A distorted square antiprismatic structure for the complex is revealed *via* single crystal X-ray diffraction analysis. In the complex, Eu(III) is coordinated to six oxygen atoms of three dbm moieties and the pyridyl and imidazolyl nitrogen atoms of impy. Steady state and time resolved photoluminescence spectra of the solid complex, its chloroform solution and its PMMA hybrid film are presented and discussed. In spite of the distorted square antiprismatic structure, the $^5D_0 \rightarrow {}^7F_2$ transition is fairly strong and the $^5D_0 \rightarrow {}^7F_0$ transition is sufficiently strong. The decay time is monoexponential for the solid complex, whereas the chloroform solution and PMMA hybrid film show biexponential decay fitting. The decay time of the $^5D_0 \rightarrow {}^7F_2$ transition of solid [Eu(dbm)₃(impy)] (417 ± 0.5 μs) is seven times longer than that of its precursor [Eu(dbm)₃(H₂O)] (57 ± 0.09 μs). The intrinsic quantum yield of the ternary complex is larger than the precursor. The solid complex and PMMA hybrid film emit a red color, while the chloroform solution emits a pink color. The simultaneous emission of white and red light results in pink.

1. Introduction

The spectrally narrow and distinctive emission from Ln(III) complexes has been appropriated for an extensive range of applications in many areas, such as being used in contrast agents for metal sensing[1,2] and MRI,[3,4] as a laser material,[5,6] in light converting molecular systems,[7,8] and for immunoassay applications.[9,10] These complexes show large Stokes shifts, high luminescence efficiency and long emitting lifetimes, which make them promising candidates for a wide range of photonic applications, such as being used in electroluminescent devices, displays and OLED devices.[11,12] It is well known that lanthanide luminescence arises from transitions within 4f orbitals. These transitions are parity-forbidden and, therefore, direct excitation is not effective and does not yield fruitful luminescence. Luminescence is most successfully achieved through a sensitizer that absorb photons and subsequently populates the states of the lanthanide ions through an intramolecular energy transfer process called the "antenna effect".[13,14] The intramolecular energy

transfer from the triplet state of the ligand to Ln(III) depends on the structure of the ligand and its triplet energy state.

The lanthanide ion in tris(β-diketonate) complexes can expand its coordination sphere through forming adducts with neutral molecules containing oxygen or nitrogen donor atoms. Since lanthanide tris(β-diketonates) are coordinatively unsaturated, the water molecules present in the neighborhood easily attach themselves to the lanthanide. This results in the quenching of the metal excited states non-radiatively, leading to a decrease in the luminescence intensity and excited-state lifetime.[15] The substitution of water molecules by neutral ancillary ligands, such as pyrazine,[16,17] 2,4,6-tris(2-pyridyl)-1,3,5-triazine,[18,19] 2,2′-bipyridyl,[20] 2,2′-bipyrimidine,[21,22] 1,10-phenanthroline,[23] *etc.*, can reduce non-radiative decay and thus strongly enhance the luminescence intensity and quantum yield.

In particular Eu(III) is a promising candidate, since it exhibits intense red photoluminescence with a long emitting lifetime[24] and high quantum yield.[25] Furthermore, [Eu(dbm)₃] ternary complexes, which are thermally very stable,[26] have shown enthralling and appealing photophysical properties.[27,28] These properties make the complexes a favorable species for the fabrication of LEDs.

The N,N-donor 2-(1*H*-imidazol-2-yl)pyridine forms complexes *via* coordinating through both the imidazolyl and pyridyl nitrogen atoms.[29,30] The impy ligand is a structurally and electronically

Lanthanide Research Laboratory, Department of Chemistry Jamia Millia Islamia, New Delhi 110 025, India. E-mail: kiftikhar@jmi.ac.in

asymmetric ligand and, upon coordination, it can create some kind of distortion in the geometry of the complex. The distorted geometry results in an asymmetric environment being created around the metal ion. The asymmetric environment may enhance luminescence from the complex. To the best of our knowledge, lanthanide complexes of 2-(1H-imidazol-2-yl)-pyridine have not been reported so far, except for one report from our laboratory.[31] A ten-coordinated [Eu(hfaa)$_3$(impy)$_2$] complex has shown reasonably enhanced luminescence and longer lifetimes.[31] This tempted us to synthesize a ternary complex of Eu(dbm)$_3$·H$_2$O with impy. In this paper, we report the synthesis, crystal structure and photophysical properties of a novel europium ternary β-diketonate: [Eu(dbm)$_3$(impy)] (dbm is the anion of dibenzoylmethane and impy is the neutral 2-(1H-imidazol-2-yl)pyridine ligand).

2. Experimental

2.1. Materials and physical measurements

The commercially available chemicals that were used without further purification are: Gd$_2$O$_3$ (99.9%); Eu$_2$O$_3$ (99.9%); 2-(1H-imidazol-2-yl)pyridine; and 1,3-diphenyl-1,3-propanedione, which were obtained from Sigma-Aldrich. The oxides were converted to their corresponding chlorides via a standard method.[22] The solvents used in this study were of AR grade.

Elemental analyses of the samples were carried out using an Elementar Modern Elemental Analyser (type: Vario EL cube). The melting points of the complexes were recorded through a conventional capillary method. Thermograms (TGA/DTA curves) were recorded under an inert atmosphere (N$_2$) at a heating rate of 10 °C min^{-1} using Exstar 6000 TGA/DTA apparatus from SIINT, Japan. Infrared spectra, as KBr discs, were recorded using a PerkinElmer spectrum RX 1 FT-IR spectrophotometer over the range of 4000 to 400 cm^{-1}. ESI-MS$^+$ data of the complexes in positive ion mode were recorded using a Waters Micromass Q-T mass spectrometer. The steady-state luminescence and excitation spectra were recorded using a Horiba Jobin Yvon Fluorolog 3-22 spectrofluorometer equipped with a 450 W xenon lamp (the excitation source) and an R928P Hamamatsu photomultiplier tube (the detector). The slit width was kept at 2 nm. The lifetimes of the complexes in the visible region were recorded using an Edinburgh FLS920 fluorescence spectrometer equipped with a Hamamatsu R5509-72 supercooled photomultiplier tube at 193 K and a TM300 emission monochromator. The electronic spectra (200–400 nm) were obtained using a PerkinElmer Lambda-40 spectrophotometer using a 1 cm^3 stoppered quartz cell with a 1 cm path length.

The intrinsic quantum yields (Q_{Ln}^{Ln}) of samples were calculated for the solid complexes and their chloroform solutions at room temperature, using the following equations:[32]

$$Q_{Ln}^{Ln} = \frac{\tau_{obs}}{\tau_{rad}} \quad (1)$$

$$\frac{1}{\tau_{rad}} = A_{MD,0} \cdot \eta^3 \left(\frac{I_{tot}}{I_{MD}} \right) \quad (2)$$

where τ_{obs} is the actual lifetime of the emitting excited state and τ_{rad} is the radiative lifetime of this state. $A_{MD,0}$ is the spontaneous emission probability for the $^5D_0 \rightarrow {^7F_1}$ transition under vacuum (14.65 s^{-1}), η is the refractive index of the solvent, and I_{tot}/I_{MD} is the ratio of the total integrated intensity of the corrected emission spectrum to the integrated intensity of the $^5D_0 \rightarrow {^7F_1}$ magnetic dipole transition of Eu(III).

2.2. X-ray crystallography

Single crystal X-ray diffraction data were collected using a Smart Lab 9 kW rotating anode X-ray diffractometer at room temperature, using a SuperNova (Mo) X-ray source and MoKα radiation (k = 0.71073 Å). Data collection and cell refinement were performed using CrysAlisPro 1.171.38.43i (Rigaku OD, 2015). Data for the structures were corrected for absorption using Gaussian integration. The structures were solved with the ShelXT (Sheldrick, 2015), using olex2 software. The structure solutions, using a direct method, were obtained with SHELXL-2016/6. The data refinement package used least squares minimization. Anisotropic parameters were refined to all non-hydrogen atoms. Hydrogen atom positions were constrained to neutral diffraction distance values.[33] Crystallographic tables were produced using OLEX2 software. Crystal structure refinement data for the complex [Eu(dbm)$_3$(impy)] is displayed in Table 1. The crystal code provide by the CCDC is 1883323.†

2.3. Syntheses of the complexes

2.3.1. Synthesis of [Ln(dbm)$_3$(H$_2$O)] (Ln = Eu and Gd). The complexes were synthesized via similar methods. The synthesis of [Eu(dbm)$_3$(H$_2$O)] given here is representative.

The complex [Eu(dbm)$_3$(H$_2$O)] was synthesized according to a published procedure[34] with some modifications. An aqueous solution of EuCl$_3$·6H$_2$O (1.8320 g; 5.0 × 10^{-3} moles) was slowly added to a continuously stirred mixture of Hdbm (2.2425 g; 0.01 moles) in ethanol and 10 mL of 1 M aqueous NaOH solution. This was stirred for 6 h after adding excess water. A yellow precipitate of the complex appeared. This was filtered, washed several times with water, and dried under vacuum over P$_4$O$_{10}$. The compound was further washed with n-hexane to remove any unreacted Hdbm. Then it was dried in air and finally under vacuum. The compound, thus finally obtained, was thoroughly characterized before use.

[Eu(dbm)$_3$(H$_2$O)]: yield: 2.80 g (69.00%); mp: 233–238 °C (lit. 230–234 °C[26]). Elemental analysis: found (%): C, 64.94; H, 4.20; required (%): C, 64.36; H, 4.17. ESI-MS$^+$ m/z: 821.0 [Eu(dbm)$_3$]$^+$, 225.0 [dbm]$^+$; IR (KBr; cm^{-1}): 3588–3200 cm^{-1}, ν(O–H); 3058 and 3028 cm^{-1}, aromatic ν_{as}(C–H) and ν_s(C–H); 1596 cm^{-1}, ν_{as}(C=O); 1550 cm^{-1}, ν_s(C=C); 1522 cm^{-1}, ν_s(C=O); 1480 cm^{-1}, δ_{as}(C–H); 1308 cm^{-1}, ν_{as}(C=C); 1226 cm^{-1}, δ_s(C–H); 754 cm^{-1}, π(C–H).

[Gd(dbm)$_3$(H$_2$O)]: Yield: 2.50 g (57.00%); mp: 249–254 °C (lit. 250–253 °C[26]). Elemental analysis: found (%): C, 64.78; H, 4.12; required (%): C, 63.95; H, 4.37.

2.3.2. Synthesis of [Ln(dbm)$_3$(impy)] (Ln = Eu and Gd). These complexes were synthesized via similar methods. The synthesis of [Eu(dbm)$_3$(impy)] given here is representative.

Table 1 Crystal data and structural refinement parameters for the complex [Eu(dbm)$_3$(impy)]

Empirical formula	C$_{53}$H$_{40}$EuN$_3$O$_6$
Formula weight	966.84
Temperature	293(2) K
Wavelength	0.71073 Å
Crystal system	Monoclinic
Space group	$P2_1/c$
a	13.1559(4) Å
b	22.4747(5) Å
c	16.1361(6) Å
α	90°
β	109.698(4)°
γ	90°
Volume	4491.8(3) Å^3
Z	4
Density (calculated)	1.430 Mg m^{-3}
Absorption coefficient	1.450 mm^{-1}
F(000)	1960
Crystal size	0.200 × 0.100 × 0.100 mm^3
Theta range for data	1.877 to 28.290°
Collection Index ranges	$-14 \leq h \leq 16$, $-23 \leq k \leq 28$, $-12 \leq l \leq 21$
Reflections collected	14 766
Independent reflections	9723
R(int)	0.0245
Completeness to theta = 25.000°	99.3%
Absorption correction	Gaussian
Max. and min. transmission	1.0 and 0.742
Refinement method	Full-matrix least-squares on F^2
Data/restraints/parameters	9723/0/573
Goodness-of-fit on F^2	1.088
Final R indices [$I > 2\text{sigma}(I)$]	R_1 = 0.0457, wR_2 = 0.1034
R indices (all data)	R_1 = 0.0659, wR_2 = 0.1158
Extinction coefficient	0.00117(14)
Largest diff. peak and hole	0.623 and -2.075 e Å^{-3}

5 mL of an ethanolic solution of impy (0.0340 g; 2.3 × 10^{-4} moles) was added dropwise into 15 mL of an ethanolic solution of [Eu(dbm)$_3$(H$_2$O)] (0.2000 g; 2.3 × 10^{-4} moles), and this was stirred using a magnetic stirrer. Finally, the complex precipitated. It was filtered off, washed with ethanol and dried under vacuum. It was recrystallized from a mixture of dichloromethane and ethanol in a 5:2 ratio.
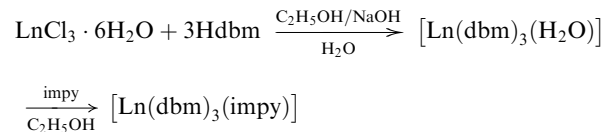
[Eu(dbm)$_3$(impy)]. Yield: 217.0 mg (94.90%); mp: 248–255 °C. Elemental analysis: found (%): C, 65.88; H, 4.15; N, 4.33; required (%): C, 65.83; H, 4.13; N, 4.31; ESI-MS$^+$ *m/z*: 967.7 [Eu(dbm)$_3$(impy) + H]$^+$, 821.7 [Eu(dbm)$_3$]$^+$, 743.7 [Eu(dbm)$_2$(impy)]$^+$, 225.0 [dbm]$^+$, 146.1 [impy]$^+$; IR (KBr; cm^{-1}): 3398 cm^{-1}, ν(N–H); 3060 and 3026 cm^{-1}, aromatic ν_{as}(C–H) and ν_s(C–H); 1598 cm^{-1}, ν_{as}(C=O); 1550 cm^{-1}, ν_s(C=C); 1518 cm^{-1}, ν_s(C=O); 1478 cm^{-1}, δ_{as}(C–H); 1308 cm^{-1}, ν_{as}(C=C); 1220 cm^{-1}, δ_s(C–H); 1024 cm^{-1}, ν(N–C–C); 748 cm^{-1}, π(C–H); 722 cm^{-1}, π(C–H).

[Gd(dbm)$_3$(impy)]. Yield: 205.0 mg (90.70%); mp: 254–260 °C. Elemental analysis: found (%): C, 66.00; H, 4.22; N, 3.94; required (%): C, 65.47; H, 4.11; N, 4.32.

3. Results and discussion

The syntheses of the [Ln(dbm)$_3$(impy)] (Ln = Eu and Gd) complexes were performed according to procedures reported

in the literature.[16] One equivalent of [Ln(dbm)$_3$(H$_2$O)] was mixed with one equivalent of impy in ethanol at room temperature, which gave the eight-coordinate [Ln(dbm)$_3$(impy)] complexes (Scheme 1). The resulting products are in accordance with the assumption that eight-coordinate complexes would be formed, since the stoichiometry was taken as [Ln(dbm)$_3$(H$_2$O)] : impy (a 1 : 1 ratio). The complexes are resistant to air and moisture, have poor solubility in common organic polar solvents like chloroform, dichloromethane, methanol and ethanol, and are insoluble in nonpolar solvents like *n*-hexane, *n*-heptane, *etc.*

$$\text{LnCl}_3 \cdot 6\text{H}_2\text{O} + 3\text{Hdbm} \xrightarrow[\text{H}_2\text{O}]{\text{C}_2\text{H}_5\text{OH/NaOH}} \left[\text{Ln(dbm)}_3(\text{H}_2\text{O})\right]$$

$$\xrightarrow[\text{C}_2\text{H}_5\text{OH}]{\text{impy}} \left[\text{Ln(dbm)}_3(\text{impy})\right]$$

3.1. The crystal structure of [Eu(dbm)$_3$(impy)]

Single crystal X-ray analysis of the complex [Eu(dbm)$_3$(impy)] indicates that the crystals are monoclinic with the space group $P2_1/c$. The unit cell has the dimensions: a = 13.1559(4) Å; b = 22.4747(5) Å; and c = 16.1361(6) Å. The crystal parameters and refinement results are listed in Table 1 and the bond distances are collected in Table S1 (ESI†).

Each unit cell contains four molecules, and each molecule consists of one Eu(III) atom, three β-diketonates (dbm) and one ancillary ligand (impy) (Fig. 1a and c). Eu(III) is eight-coordinated and has distorted square antiprismatic geometry. This distorted square antiprismatic structure is due to the coordination of six oxygen atoms (O$_1$, O$_2$, O$_3$, O$_4$, O$_5$ and O$_6$) from three bidentate dbm ligands and two nitrogen atoms (N$_1$ and N$_3$) from one bidentate impy ligand, making an EuO$_6$N$_2$ polyhedron (Fig. 1b). The central Eu(III) atom in this asymmetric unit is, thus, saturated by the three anionic aromatic dbm ligands and one neutral ancillary impy ligand, leading to an encapsulated structure. It, therefore, meets the structural requirements for an efficient lanthanide luminescent material by protecting Eu(III) from vibrational coupling and increasing the light absorption cross-section *via* the so-called "antenna effect". The Eu–O bond length range (Table S1, ESI†) is in agreement with the bond lengths reported for other β-diketonate complexes.[13] The average Eu–N bond length of 2.59 Å for the complex [Eu(dbm)$_3$(impy)] is close to the mean value of 2.60 Å found for [EuO$_6$N$_2$]-containing complexes available in the Cambridge Crystallographic Database.[35] In the six-membered chelating ring, the C–O bond length varies between 1.254 and 1.280 Å, and that of C–C varies between 1.388 and 1.399 Å. These data suggest strong conjugation within this five-member electron loop. Selected bond distances and angles are listed in Table S1 (ESI†).

Semi-quantitative polytopal analysis has demonstrated that an eight-coordinated complex may be a square antiprism (SAP)-D$_{4d}$, dodecahedron (DD)-D$_{2d}$, or bicapped trigonal prism (BTP)-C$_{2v}$.[36–38] For a calculation of the dihedral angles (δ and ϕ), all the donor atoms (six oxygen and two nitrogen atoms) were arranged within six planes (Fig. S1, ESI†). The values
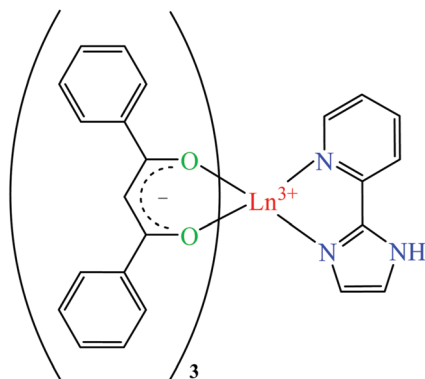
Ln = Eu and Gd

Scheme 1 The synthesis of the [Ln(dbm)₃(impy)] complexes.

of δ and ϕ are summarized in Table 2. The dihedral angles δ_1 (1.69°) and δ_2 (14.82°) for the complex reveal that the squares are close to planarity. Furthermore, the δ_3 and δ_4 values are 54.98° and 58.53°, respectively, and ϕ_1 and ϕ_2 are 30.14° and 27.63°, respectively. These values show proximity to the ideal values of a square antiprism (SAP) (Table 2). This suggests slightly distorted square antiprismatic geometry.

3.2. IR spectra

Infrared spectra of [Eu(dbm)₃(H₂O)], [Eu(dbm)₃(impy)], Hdbm and impy are shown in Fig. 2. The assignments are made through comparison with reported related compounds. The spectrum of

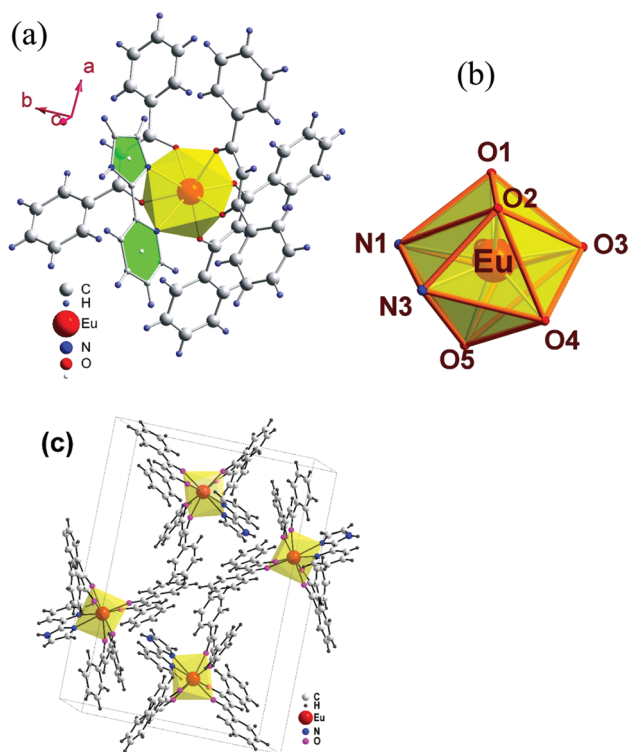**Fig. 1** (a) The molecular structure of the eight-coordinate [Eu(dbm)₃(impy)] complex; (b) the coordination geometry around Eu(III); and (c) the unit cell.

Table 2 The values of the dihedral angles δ and φ in degrees

		SAP	BTP	DD
δ_1	O4–[O5–O3]–O6[a]	1.6	0.0	0.0	29.5
δ_2	N3–[N1–O2]–O1[a]	14.8	0.0	21.8	29.5
δ_3	N1–[O5–N3]–O4[a]	54.9	52.4	48.2	29.5
δ_4	O2–[O3–O1]–O6[a]	58.5	52.4	48.2	29.5
φ_1| O3–N1–O4–N3[b]	30.1	24.5	14.1	0.0
φ_2| O5–O2–O6–O1[b]	27.6	24.5	14.1	0.0

[a] $A[BC]D$ is the dihedral angle between the ABC plane and the BCD plane. [b] A–B–C–D is the dihedral angle between the $(AB)CD$ plane and the $AB(CD)$ plane, where (AB) is the center of A and B.

free impy shows a band at 1588 cm⁻¹, which is attributed to a C=N stretching frequency, probably somewhat coupled with a pyridine ring vibration (1594–1566 cm⁻¹).[39] The strong broad band due to an N–H stretching vibration, coupled with the C–H stretching, of free impy appears in the region of 3200–2500 cm⁻¹. This has been transformed into a relatively weaker band upon coordination, which can be seen in the IR spectrum of [Eu(dbm)₃(impy)]. This reflects the coordination of impy to Eu(III). An O–H stretching vibration appearing as a broad band in the region of 3500–3290 cm⁻¹ in the IR spectrum of [Eu(dbm)₃(H₂O)] has disappeared from the IR spectrum of [Eu(dbm)₃(impy)], and this is strong evidence that impy has replaced the water molecule. All the IR bands characteristic of dbm present in [Eu(dbm)₃(H₂O)] are also present in [Eu(dbm)₃(impy)], with their positions shifted.

3.3. Mass spectra

ESI-MS spectra in positive ion mode for [Eu(dbm)₃(H₂O)] and [Eu(dbm)₃(impy)] were obtained in chloroform solution (Fig. S2, ESI†). The spectrum of [Eu(dbm)₃(H₂O)] does not show an intact molecular ion peak, however, the spectrum displays a strong peak at m/z = 225.0, which is assigned to a [dbm]⁺ moiety, and the peak retrieved at m/z = 821.0 represents the six coordinate species [Eu(dbm)₃]⁺. This indicates that the water molecule inside the coordination sphere is loosely bonded. The spectrum of [Eu(dbm)₃(impy)] shows a weak intact molecular ion peak for [Eu(dbm)₃(impy) + H]⁺ at m/z = 967.7. In addition, a strong peak at m/z = 146.1 indicates the presence of [impy]⁺. The peak at m/z = 743.7 is assigned to [Eu(dbm)₂(impy)]⁺, and the peak at m/z = 821.0 is assigned to [Eu(dbm)₃]⁺. The other peaks observed in the spectrum may represent the diverse ionic species formed due to fragmentation, ligand exchange and redistribution in the vapor phase.[40,41]

3.4. Thermal analysis

The thermal stability of lanthanide complexes is an important factor in the fabrication of electroluminescent devices.[42] Thermograms of [Eu(dbm)₃(H₂O)] and [Eu(dbm)₃(impy)] (Fig. 3) are recorded over the range from ambient temperature to 900 °C. The TGA curve of [Eu(dbm)₃(H₂O)] shows a first weight loss of 2.1% at 101 °C; this corresponds to the removal of one water molecule (the theoretical weight loss for one water molecule is 2.09%). Further decomposition steps are observed over the temperature ranges of 202–392, 392–568 and 568–867 °C, with corresponding weight losses of 30.95, 26.70 and 19.67%.
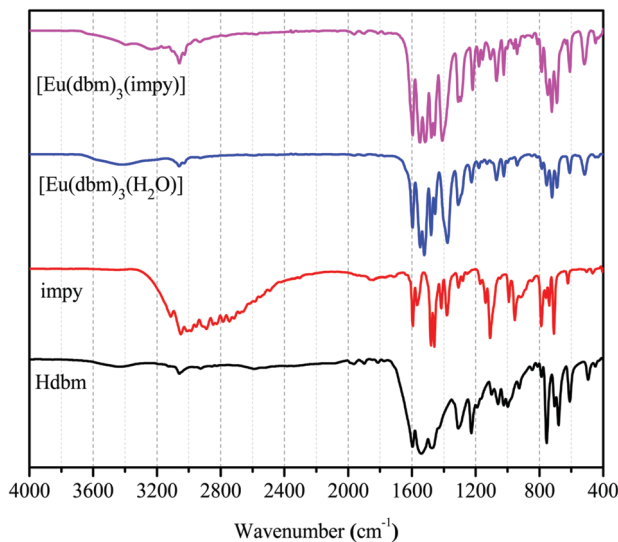
Fig. 2   IR spectra of Hdbm, impy, [Eu(dbm)$_3$(H$_2$O)] and [Eu(dbm)$_3$(impy)].

Fig. 3   Thermograms of (a) [Eu(dbm)$_3$(H$_2$O)] and (b) [Eu(dbm)$_3$(impy)].

These represent the removal of dbm units in three steps (the theoretical weight loss for one dbm unit is 26.02%). The DTA curve displays one strong endothermic peak at 235 °C, which represents the melting of the complex.

The thermogram of [Eu(dbm)$_3$(impy)] does not show any weight loss up to 205 °C, which reflects that the complex is anhydrous. Decomposition begins at 220 °C. The first weight loss, of 44.5%, is observed over the temperature range of 205–460 °C. This represents the expulsion of two dbm moieties (the theoretical weight loss for two dbm moieties is 46.22%). The next step reflects the simultaneous removal of one moiety of dbm and an impy unit over the temperature range from 460 to 779 °C. The weight loss noted for this expulsion is 40.3% (the theoretical weight loss for one dbm unit and one impy unit is 38.14%). The DTA curve shows one endothermic peak at 254 °C, which represents the melting point of the complex.

3.5. Absorption spectra

UV absorption spectra of Hdbm, impy, [Eu(dbm)$_3$(H$_2$O)] and [Eu(dbm)$_3$(impy)] are summarized in Fig. S3 (ESI†). Free impy shows maximum absorption at 297 nm, which corresponds to a π–π* transition.[29] The absorption spectrum of Hdbm shows two bands at 342 and 253 nm, which are attributed to π–π* transitions; these are assigned to S$_0$ → S$_1$ and S$_0$ → S$_2$ transitions, respectively.[43] The absorption spectra of [Eu(dbm)$_3$(H$_2$O)] and [Eu(dbm)$_3$(impy)] are dominated by the absorption of Hdbm, however, the presence of impy could be seen in the form of a very weak shoulder at 298 nm in the case of [Eu(dbm)$_3$(impy)], which suggests the coordination of impy with [Eu(dbm)$_3$(H$_2$O)]. The higher molar extinction coefficient of [Eu(dbm)$_3$(impy)] (5.73×10^4 L mol^{-1} cm^{-1}) compared to [Eu(dbm)$_3$(H$_2$O)] (5.03×10^4 L mol^{-1} cm^{-1}) provides strong evidence for the coordination of impy to Eu(III).

4. Phosphorescence

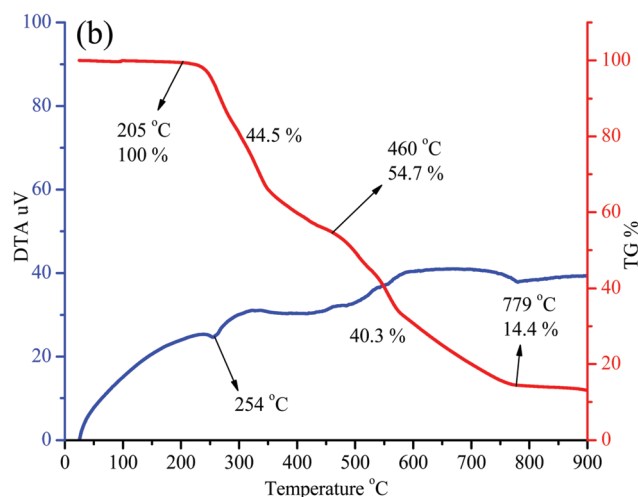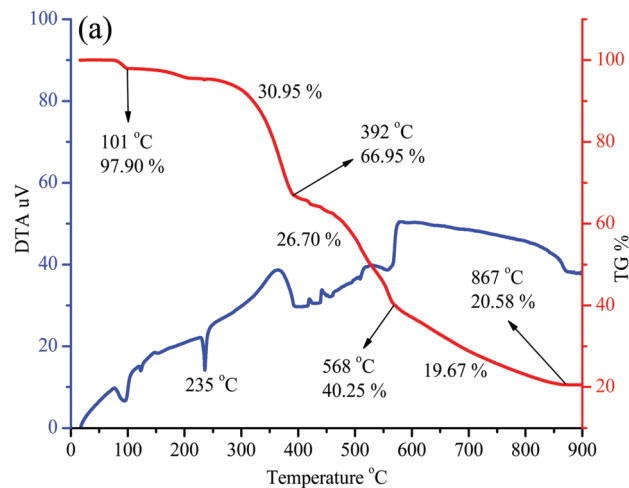It is important to determine the energy of the triplet state of ligands. The triplet state of a ligand plays an important role in influencing the luminescence. Usually, Gd(III) complexes are used to elucidate the energy of the triplet state because the emitting state ($^6P_{7/2}$) of Gd(III) lies at too high of an energy (33 333 cm^{-1}) to be populated through organic ligands.[44] In addition, they have a larger probability for ligand phosphorescence because of the combination of both paramagnetic and heavy-atom effects.[45] Here, to find out the energy of the triplet state of the ligands (dbm and impy), the phosphorescence spectrum of [Gd(dbm)$_3$(impy)] was recorded at 77 K in dichloromethane (λ_{ex} = 275 nm) (Fig. 4). The spectrum shows two maxima centered at 20 429 and 19 120 cm^{-1}. Since the maximum at 20 429 cm^{-1} corresponds to $E_{T(0-0)}$ dbm,[46] therefore, the other maximum at 19 120 cm^{-1} could safely be assigned to the energy of the triplet state of impy.

5. Photoluminescence

Excitation spectra in the solid state, in chloroform solution and from hybrid films of [Eu(dbm)$_3$(H$_2$O)] (Fig. S4, ESI†) and [Eu(dbm)$_3$(impy)] (Fig. 5) were recorded at 300 K. The excitation spectra were obtained by monitoring the position
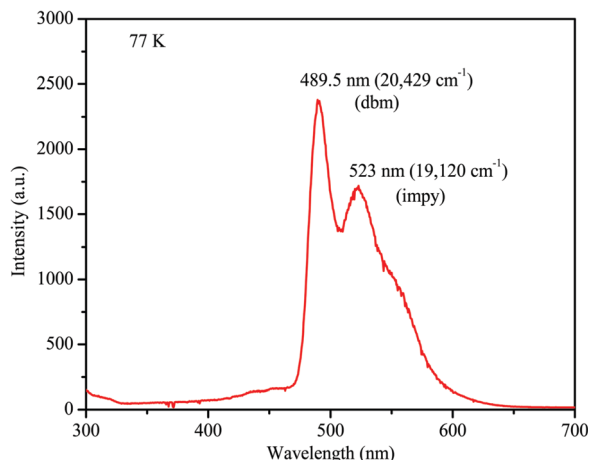
Fig. 4 The phosphorescence spectrum of [Gd(dbm)$_3$(impy)] at 77 K.

of $^5D_0 \rightarrow {}^7F_2$ emission. These spectra contain a broad band that correspond to the excitation of the ligands (S$_0 \rightarrow$ S$_1$). The excitation spectra of the hybrid films do not show f–f transitions, which reflects the efficient ligand to metal energy transfer.

The photoluminescence spectra of [Eu(dbm)$_3$(impy)] and [Eu(dbm)$_3$(H$_2$O)] were recorded in the solid state, in chloroform solution and from hybrid films in a PMMA polymer matrix (6.0% wt/wt) at 300 K (Fig. 6 and Fig. S5, ESI†). The triplet state of dbm lies at 20 429 cm^{-1} and that of impy lies at 19 120 cm^{-1}. The energy of the $^5D_0$ emitting level of Eu(III) is 17 500 cm^{-1}.[44] This reflects that the triplet states of dbm and impy lie,

respectively, 2929 and 1620 cm^{-1} above the $^5D_0$ emitting level of Eu(III) (Fig. 7). The energy difference of 2929 cm^{-1} between $E_{triplet}$ of dbm and the $^5D_0$ emitting level of Eu(III) is ideal for efficient energy transfer from dbm.[44] The energy difference of 1620 cm^{-1} between the triplet state of impy and the emitting $^5D_0$ level is lower than the optimum energy difference.[44] This small difference may facilitate the probability of back energy transfer. The energy difference between the triplet states of dbm and impy is 1309 cm^{-1}, which is close to the energy difference between E_T of dbm and the $^5D_1$ level of Eu(III) (1429 cm^{-1}). These values are much lower than the optimum energy difference required to allow energy transfer effectively.[44] It appears that energy transfer from dbm to impy or the $^5D_1$ level of Eu(III) has equal probability.

It is interesting to note that the emission spectra of solid [Eu(dbm)$_3$(impy)] and the polymer film do not show any ligand-centered emission in the region 350–450 nm. This is the result of efficient ligand to metal energy transfer.

The luminescence spectra of chloroform solutions of the complexes display five characteristic ^7F_j emission peaks ($j = 0$, 1, 2, 3, 4) originating from the $^5D_0$ emitting state of Eu(III). The luminescence spectra of both complexes are dominated by a sharp induced electric-dipole ($^5D_0 \rightarrow {}^7F_2$) transition, which is responsible for the intense red luminescence of the complexes [Eu(dbm)$_3$(H$_2$O)] and [Eu(dbm)$_3$(impy)].[47–49] The spectra of solid [Eu(dbm)$_3$(impy)] and its hybrid film show six expected peaks, five from $^5D_0 \rightarrow {}^7F_{0–4}$ and one from $^5D_1 \rightarrow {}^7F_1$.[50,51] However, for [Eu(dbm)$_3$(H$_2$O)], the transition $^5D_1 \rightarrow {}^7F_1$ could

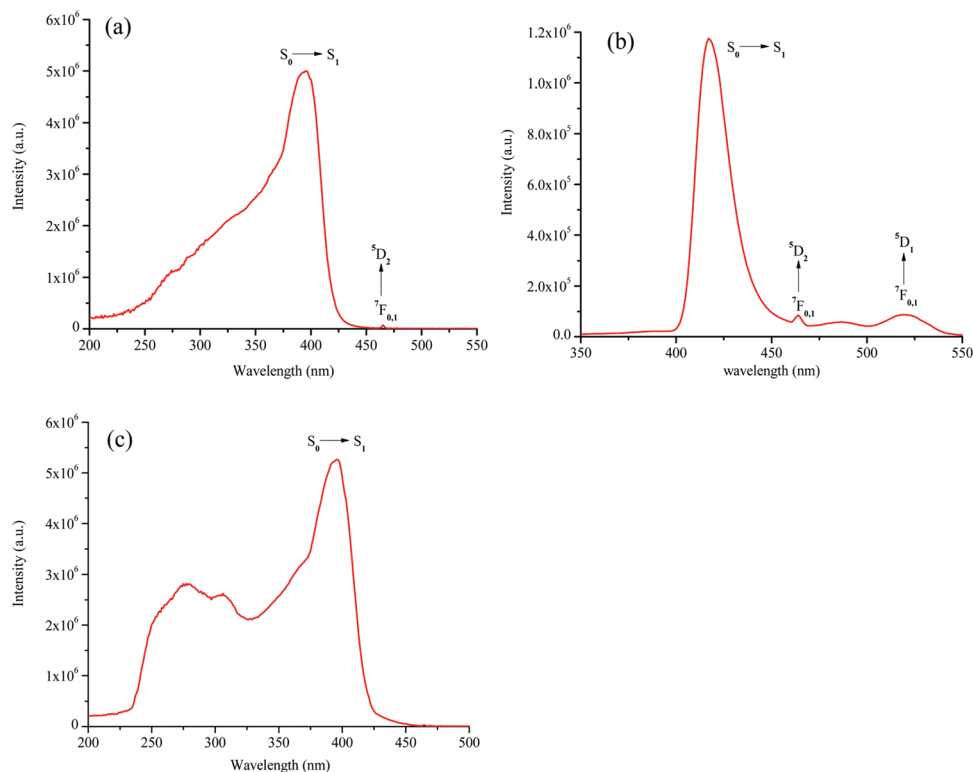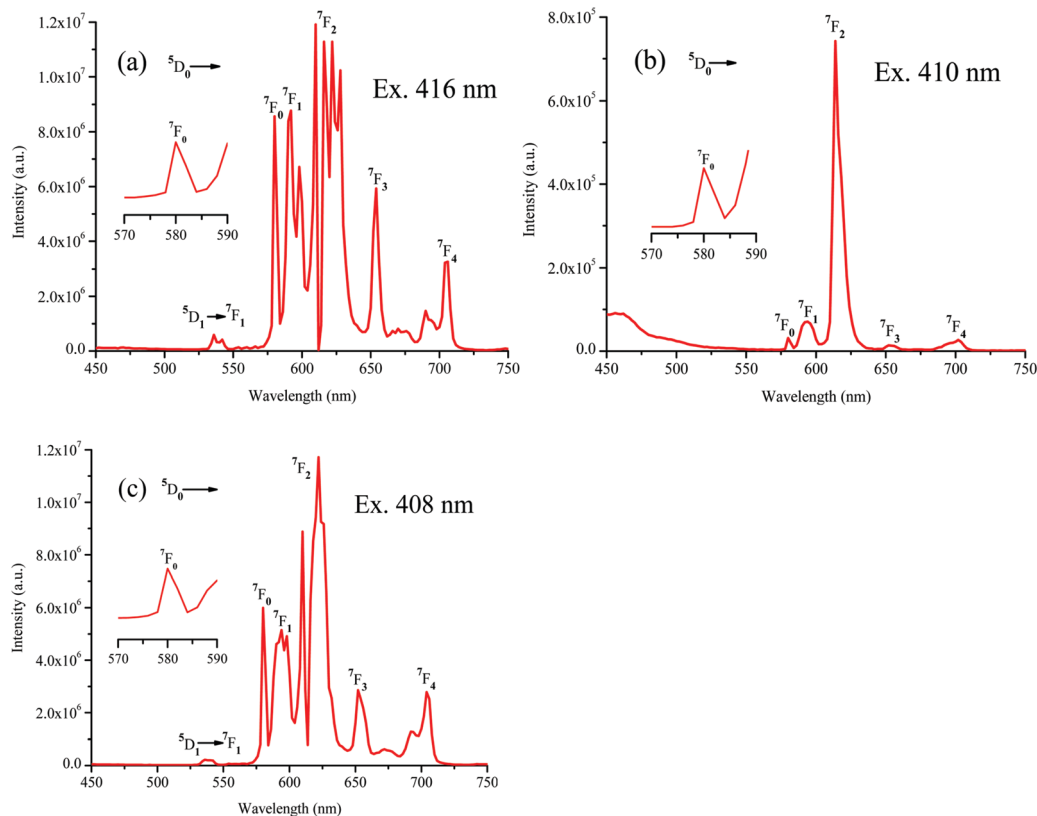**Fig. 5** Excitation spectra of [Eu(dbm)$_3$(impy)] (a) in the solid state, (b) in chloroform, and (c) as a hybrid film.

Fig. 6   Emission spectra of [Eu(dbm)$_3$(impy)] (a) in the solid state, (b) in chloroform, and (c) as a hybrid film.

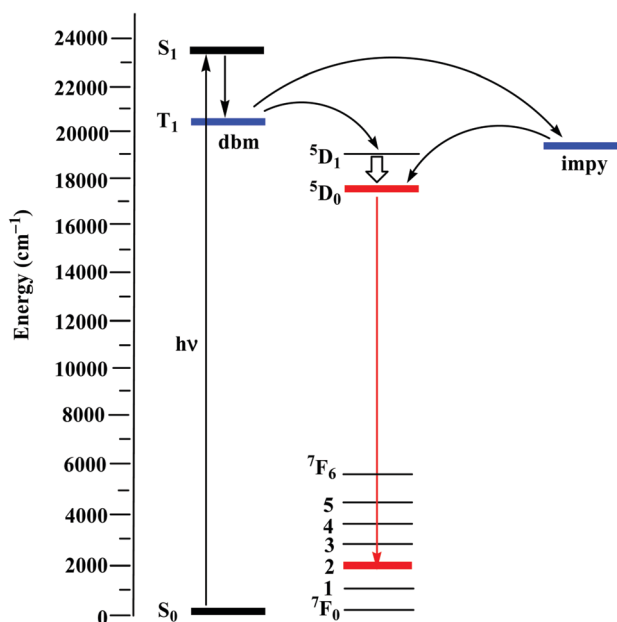Fig. 7   An energy level diagram of the ligands and Eu(III) in [Eu(dbm)$_3$(impy)].

not be obtained. The transition $^5D_0 \rightarrow {}^7F_2$ is hypersensitive and its intensity is reasonably influenced by the environment around Eu(III) (ligands and solvents) and the geometry of the complex. It could be split into many components due to the

Stark effect.[52] This transition is highly split and the Stark components are striking in the case of the solid complex. In the case of the hybrid film, although it is well split, the number of Stark components is much lower than in the spectrum of the solid. Although the emission intensity of the $^5D_0 \rightarrow {}^7F_1$ magnetic-dipole transition does not depend on the chemical environment around europium, the splitting of this transition into Stark components tells us about the unsymmetrical site symmetry around europium.[24] In the case of [Eu(dbm)$_3$(impy)], this transition ($^5D_0 \rightarrow {}^7F_1$) shows Stark splitting and appears as a doublet, both in the solid state and in the hybrid film. This clearly indicates the asymmetric environment around Eu(III), and is in agreement with the distorted square antiprismatic crystal structure of the complex. A singlet existing for the $^5D_0 \rightarrow {}^7F_0$ electric-dipole transition indicates the single site symmetry of Eu(III) in every phase.[53] This corroborates with the single crystal structure results.

The values of the luminescence intensity ratio (R) and the full width at half maximum (FWHM) are summarized in Table 3. The $^5D_0 \rightarrow {}^7F_J$ (J = 0, 2, 4) forced electric-dipole transitions are very sensitive to the environment around europium and their intensities depend upon the symmetry of the complex. In a low site symmetry complex, these transitions gain intensity. However, the magnetic-dipole transitions $^5D_0 \rightarrow {}^7F_1$ and $^5D_0 \rightarrow {}^7F_3$ are independent of the surrounding environment. Therefore, the ratio R could give valuable information regarding changes in the environment around Eu(III). The values of R in

Table 3 The luminescence intensity ratios and FWHM values of the complexes

	[Eu(dbm)$_3$(H$_2$O)]		[Eu(dbm)$_3$(impy)]	
	R	FWHM (nm)	R	FWHM (nm)
Solid	8.32	3.73	2.15	2.82
Solution (CHCl$_3$)	7.04	5.57	6.77	10.15
Hybrid film	9.72	8.23	2.37	12.52

R is the intensity ratio of the transitions $^5D_0 \rightarrow {}^7F_2$ and $^5D_0 \rightarrow {}^7F_1$.

the case of solid [Eu(dbm)$_3$(impy)] and its hybrid film are relatively much lower than for recently reported asymmetric complexes.[48,54,55] Since the complex has distorted square anti-prismatic geometry, therefore it is highly asymmetric, with the absence of an inversion center. The low value of R is due to the intensity of the $^5D_0 \rightarrow {}^7F_1$ magnetic-dipole transition being relatively high, which could be due to the crystal field induced mixing of the $^7F_3$ and $^7F_0$ states with components of the $^7F_2$ state.[56]

The $^5D_0 \rightarrow {}^7F_2$ transition is forbidden under D$_4$d (SAP) geometry and the intensity of this transition is expected to be weak.[57] However, this transition is strong with prominent Stark splitting in the solid as well as in the hybrid film of the present complex due to J-mixing.[58] Generally, mixing of the $^7F_0$ and $^7F_3$ states with components of $^7F_2$ is known as J-mixing.[56] The luminescence spectra of compounds with D$_4$d symmetry are dominated by the $^5D_0 \rightarrow {}^7F_4$ transition while the $^5D_0 \rightarrow {}^7F_2$ transition is forbidden. However, it is interesting to note that, in the case of the present complex, the $^7F_2$ transition is quite intense in spite of the D$_4$d symmetry of the complex, and the $^7F_4$ transition is also relatively much more intense in the solid state and hybrid film luminescence spectra compared to the solution spectrum. The intensity gain of the $^7F_4$ transition could be related to the absence of a center of symmetry in the complex. The $^5D_0 \rightarrow {}^7F_0$ transition is strictly forbidden according to Judd–Ofelt theory. Nevertheless, this transition is observed with high intensity in the solid sample and the hybrid film of the present Eu(III) complex. This transition gains intensity most probably through J-mixing or the mixing of low-lying charge-transfer states into a wavefunction with a 4f^6 configuration.[24] The $^5D_0 \rightarrow {}^7F_1$ and $^5D_0 \rightarrow {}^7F_3$ transitions, according to Judd–Ofelt theory, are forbidden and become allowed through magnetic-dipole selection rules; therefore, the intensities of these transitions are expected to be very weak. However, in the case of the present complex, these transitions ($^5D_0 \rightarrow {}^7F_1$ and $^5D_0 \rightarrow {}^7F_3$) are sufficiently strong. These transitions gain intensity via J-mixing, which permits the borrowing of intensity from the $^5D_0 \rightarrow {}^7F_2$ electric dipole transition.[24,56]

The intensities of the $^5D_0 \rightarrow {}^7F_j$ (j = 0, 1, 2, 3 and 4) transitions in the solid complex and its hybrid film are very high and follow the order: $^7F_2 > {}^7F_1 > {}^7F_0 > {}^7F_3 > {}^7F_4$ and $^7F_2 > {}^7F_1 > {}^7F_4 > {}^7F_0 > {}^7F_3$, respectively. The $^5D_0 \rightarrow {}^7F_3$ transition is more intense in the solid, which is a sign of stronger J-mixing in comparison to the hybrid film, which is in good agreement with the number of Stark components

present in the $^5D_0 \rightarrow {}^7F_2$ transition. The larger the number of Stark components in the $^7F_2$ peak, the stronger the J-mixing is. The intensities of the emission transitions in the solution spectrum follow a similar trend as in the hybrid film. However, the intensities of the transitions of the hybrid film are almost 100 times stronger than those noted for the solution spectrum. This means that these hybrid film transitions are much more influenced by J-mixing in comparison to the solution. The intensity of the $^5D_0 \rightarrow {}^7F_1$ magnetic-dipole transition is independent of the environment. It appears as a strong doublet for the solid [Eu(dbm)$_3$(impy)] and its hybrid film, which reflects that the intensity is influenced by J-mixing. The $^5D_0 \rightarrow {}^7F_1$ transition gains intensity due to J-mixing in the solid complex and the hybrid film. Since the $^5D_0 \rightarrow {}^7F_1$ transition is very intense for the solid complex and the hybrid film, therefore, the value of the luminescence intensity ratio (R) is very small in the solid and the hybrid film compared to in solution, which means that the complex is not highly symmetric, while it also indicates that the $^5D_0 \rightarrow {}^7F_1$ transition is highly influenced by J-mixing due to high asymmetry in the complex.

The FWHM values of the $^5D_0 \rightarrow {}^7F_2$ electric-dipole transition of [Eu(dbm)$_3$(H$_2$O)] are 3.73, 5.57 and 8.23, and for [Eu(dbm)$_3$(impy)] they are 2.82, 10.15 and 12.52 for the solid, in solution and as a hybrid film, respectively. The FWHM is narrower in the solid state for both the complexes, indicating the higher potential for these materials to be used in optoelectronic devices.

6. Lifetime and quantum yield analyses

Lifetime measurements were made at 300 K (Fig. S6, ESI†). The decay times and intrinsic quantum yields are listed in Table 4. The exponential decay fitting was performed using Origin 8.5. The decay curves of solid [Eu(dbm)$_3$(impy)] and [Eu(dbm)$_3$(H$_2$O)] are well fitted monoexponentially and they suggest mono-centric luminescence from these solid complexes. The decay curves of chloroform solutions of [Eu(dbm)$_3$(impy)] and [Eu(dbm)$_3$(H$_2$O)] and their hybrid films are biexponential. The biexponential decay of the $^5D_0 \rightarrow {}^7F_2$ transition and the singlet appearance of the $^5D_0 \rightarrow {}^7F_0$ transition suggest that two chemically different microenvironments exist around Eu(III).[59] The decay time (417 ± 0.5 μs) of the $^5D_0 \rightarrow {}^7F_2$ transition of solid [Eu(dbm)$_3$(impy)] is more than seven times that of the lifetime of the same transition for solid [Eu(dbm)$_3$(H$_2$O)] (57 ± 0.09 μs), whereas it is comparable with the lifetime reported for the analogue [Eu(dbm)$_3$(phen)] (480 μs).[60] The longer decay time for the transition of [Eu(dbm)$_3$(impy)] is a

Table 4 Decay times and quantum yields of the complexes

	[Eu(dbm)$_3$(H$_2$O)]		[Eu(dbm)$_3$(impy)]	
	Lifetime (μs)	Q (%)	Lifetime (μs)	Q (%)
Solid	57(±0.9)	3.44	417(±0.5)	9.0
Solution (CHCl$_3$)	τ_1 43(±0.4)	2.78	τ_1 51(±1.1)	4.12
	τ_2 150(±1.1)		τ_2 155(±2.2)	
Hybrid film	τ_1 85(±0.5)	—	τ_1 212(±3.5)	—
	τ_2 270(±7.3)		τ_2 554(±3.2)	

result of the coordination of impy and its occupancy position in the inner coordination sphere upon replacing the water molecule. The O–H oscillators of H_2O are responsible for decreasing the decay time of the transition in the case of $[Eu(dbm)_3(H_2O)]$. The lifetime (109 µs) of this transition for $[Eu(dbm)_3(impy)]$ in solution is longer than for $[Eu(dbm)_3(phen)]$ (80 µs).[60] The average lifetime of the $^5D_0 \rightarrow {}^7F_2$ transition for the hybrid film of $[Eu(dbm)_3(impy)]$ is more than 100% longer than the lifetime of the same transition for the hybrid film of $[Eu(dbm)_3(H_2O)]$. The reason for this appears to be similar to that suggested for the solid complexes. The lifetime of this transition is longer than $[Eu(dbm)_3(biq)]$ ($t_1 = 98$; $t_2 = 323$ µs) and is comparable to those for $[Eu(dbm)_3(phen)]$ (493 µs), $[Eu(dbm)_3(DB\text{-}bpy)]$ (454 µs) and $[Eu(dbm)_3(DN\text{-}bpy)]$ (486 µs).[59] The longest $^5D_0 \rightarrow {}^7F_2$ decay time is noted for the hybrid film of the impy complex under study. The relatively rigid structure of $[Eu(dbm)_3(impy)]$ embedded in a PMMA polymer matrix restricts the vibrations of the ligands, which results in a decrease in the number of non-radiative transitions and thus an increase in the decay time. The lifetime of this transition follows the order: hybrid film > solid complex > solution. The average lifetimes for biexponential decay were calculated using the following equation:[61]

$$\langle \tau \rangle = \frac{A_1 \tau_1^2 + A_2 \tau_2^2}{A_1 \tau_1 + A_2 \tau_2} \tag{3}$$

where, τ_1 and τ_2 are the decay times for the exponential components, and A_1 and A_2 are fitting parameter constants.

The intrinsic quantum yield was measured using the following equations:[32]

$$Q_{Eu}^{Eu} = \frac{\tau_{obs}}{\tau_{rad}} \tag{4}$$

$$\frac{1}{\tau_{rad}} = A_{MD,0} \cdot \eta^3 \left(\frac{I_{tot}}{I_{MD}} \right) \tag{5}$$

where τ_{obs} is the actual lifetime of the emitting excited state and τ_{rad} is the radiative lifetime of this state. $A_{MD,0}$ is the spontaneous emission probability for the $^5D_0 \rightarrow {}^7F_1$ transition under vacuum (14.65 s^{-1}), η is the refractive index of the solvent, and I_{tot}/I_{MD} is the ratio of the total integrated intensity of the corrected complex emission spectrum to the integrated intensity of the $^5D_0 \rightarrow {}^7F_1$ magnetic dipole transition.

The intrinsic quantum yield of solid $[Eu(dbm)_3(impy)]$ (9.0%) is approximately 100% higher that that of the chloroform solution (4.41%). The lower quantum yield in solution could be related to the quenching of triplet excited state energy by dipole–dipole coupling of the ligands (dbm and impy) with solvent molecules.[62] The intrinsic quantum yields of the solution and solid complexes are higher for $[Eu(dbm)_3(impy)]$ than $[Eu(dbm)_3(H_2O)]$. This is due to the substitution of water molecules by impy. The quantum yield of the solid complex is higher than the quantum yield of the chloroform solution. The quantum yield of $[Eu(dbm)_3(impy)]$ is not satisfactorily high when compared to an analogue phen complex, $[Eu(dbm)_3(phen)]$.[63] This could be due to the lower triplet state and the presence of an N–H oscillator in impy (the rigidly planar phen has no such oscillator).[46]

The N–H oscillator comes together with a scissoring motion. The impact of the scissoring motion of a flexible ligand on the spectra of lanthanides is reported in the literature.[64]

The radiative lifetimes were calculated using the equation:

$$A_{rad} = \frac{1}{\tau_{rad}} \tag{6}$$

and the radiative decay rate values (A_{rad}) are 2.63 ms (solution) and 2.60 ms (solid) for $[Eu(dbm)_3(H_2O)]$ and 2.76 ms (solution) and 5.80 ms (solid) for $[Eu(dbm)_3(impy)]$.

7. CIE color diagram

The CIE color coordinates (x_e, y_e) of $[Eu(dbm)_3(impy)]$ are obtained from emission spectra in different phases (Fig. 8). The values found are $x_e = 0.62$, $y_e = 0.36$; $x_e = 0.42$, $y_e = 0.21$; and $x_e = 0.63$, $y_e = 0.36$, for the solid complex, its chloroform solution and a hybrid film in a PMMA polymer matrix, respectively. The obtained values are summarized in Table 5. The CIE color coordinates indicate that $[Eu(dbm)_3(impy)]$ displays a pink color in solution. A pink color generally results from the dilution of red with a lot of white light.[65] This indicates that the emission of red light is accompanied by a large amount of white light in the solution phase. The solid and the hybrid film show a pure red color. The change in the emission color from red (solid and hybrid film) to pink (solution) could be related to the various energy transfer processes and the symmetry around the metal ion.[66] A highly asymmetric field existing around Eu(III) in the cases of the solid complex and hybrid film, which is reflected by the Stark splitting of the $^5D_0 \rightarrow {}^7F_2$ transition,
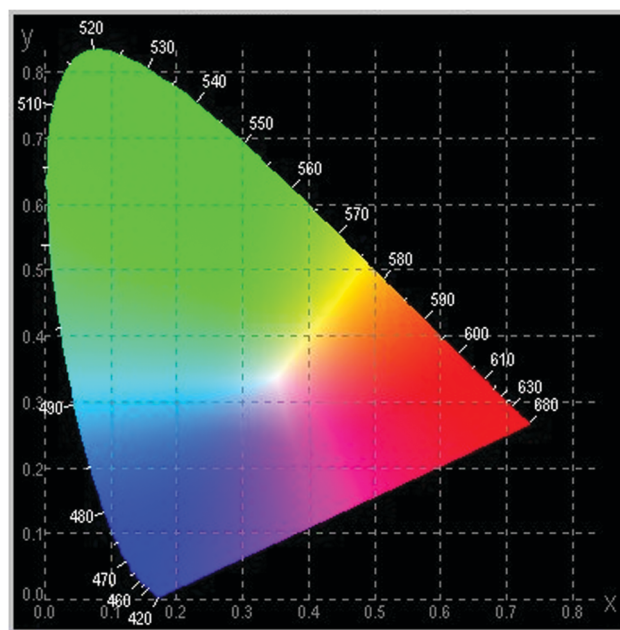
Fig. 8 The positions of the color spots of $[Eu(dbm)_3(impy)]$ in different phases in terms of the CIE chromaticity coordinates (x_e, y_e) where a: solid; b: chloroform solution; and c: hybrid film.

Table 5 CIE chromaticity coordinates (x_e, y_e) and the corresponding colors in different phases

[Eu(dbm)$_3$(impy)]	CIE coordinates		Color region
	x_e	y_e	
Solid (a)	0.62	0.36	Red
Chloroform (b)	0.42	0.21	Pink
Film (c)	0.63	0.36	Red

compared to a relatively symmetric field existing around Eu(III) in solution is the reason for the change of color.

8. Conclusions

The reaction of [Eu(dbm)$_3$(H$_2$O)] and impy in ethanol leads to the formation of an octa-coordinated [Eu(dbm)$_3$(impy)] complex. Single crystal X-ray analysis was used to establish the distorted square antiprismatic geometry of the octa-coordinate complex. The thermal stability of the complex is good, since it is stable up to 205 °C, which makes it suitable for the fabrication of LEDs. The $^5D_0 \rightarrow {}^7F_2$ transition is expected to be forbidden in distorted D$_4$d structures,[57] however, this transition is fairly strong with prominent Stark splitting in the solid complex as well as in the hybrid film. This is due to the mixing of two different states with different J values.[67] The electric-dipole $^5D_0 \rightarrow {}^7F_0$ transition is sufficiently strong in the solid complex and polymer film. The lifetime of [Eu(dbm)$_3$(impy)] is longer than [Eu(dbm)$_3$(H$_2$O)] in each phase, indicating efficient energy transfer from the triplet state of impy to the emitting level of Eu(III). The decay time of the $^5D_0 \rightarrow {}^7F_2$ transition of the hybrid film of the complex is the longest, followed by the solid complex and then the chloroform solution. The CIE chromaticity results show that the solid complex and the hybrid film emit a red color, whereas the chloroform solution emits a pink color. The pink color emission indicates that both red and white light are emitted simultaneously and the mixing of white light dilutes the red, leading to pink.

Conflicts of interest

There are no conflicts to declare.

Acknowledgements

References

1 E. L. Que and C. J. Chang, *J. Am. Chem. Soc.*, 2006, **128**, 15942–15943.

2 W. M. Wang, H. X. Zhang, S. Y. Wang, H. Y. Shen, J. Y. Zou, H. L. Gao and J. Z. Cui, *Inorg. Chim. Acta*, 2016, **442**, 172–177.

3 H. Shokrollahi, *Mater. Sci. Eng., C*, 2013, **33**, 4485–4497.

4 Y.-D. Xiao, R. Paudel, J. Liu, C. Ma, Z.-S. Zhang and S.-K. Zhou, *Int. J. Mol. Med.*, 2016, **38**, 1319–1326.

5 P. K. Shahi, A. K. Singh, S. B. Rai and B. Ullrich, *Sens. Actuators, A*, 2015, **222**, 255–261.

6 K. Nouri, *Handbook of Lasers in Dermatology*, 2014.

7 S. Xu, M. Liu, H. L. Han, Z. F. Li, Q. H. Jin, J. Hou, W. Su, Y. Y. Chen and J. Y. Yao, *Polyhedron*, 2015, **85**, 69–75.

8 L. Sun, Y. Qiu, T. Liu, J. Feng, W. Deng and L. Shi, *Luminescence*, 2015, **30**, 1071–1076.

9 H. Päkkilä, E. Malmi, S. Lahtinen and T. Soukka, *Biosens. Bioelectron.*, 2014, **62**, 201–207.

10 O. A. Goryacheva, N. V. Beloglazova, A. M. Vostrikova, M. V. Pozharov, A. M. Sobolev and I. Y. Goryacheva, *Talanta*, 2017, **164**, 377–385.

11 L. Shen, L. Yang, Y. Fan, L. Wang and J. Xu, *CrystEngComm*, 2015, **17**, 9363–9369.

12 H. Nakanotani, T. Higuchi, T. Furukawa, K. Masui, K. Morimoto, M. Numata, H. Tanaka, Y. Sagara, T. Yasuda and C. Adachi, *Nat. Commun.*, 2014, **5**, 4016.

13 K. Binnemans, *Handbook on the Physics and Chemistry of Rare Earths*, 2005, pp. 107–272.

14 H. Jeong, B. Il Lee and S. H. Byeon, *ACS Appl. Mater. Interfaces*, 2016, **8**, 10946–10953.

15 G. E. Buono-core, H. Li and B. Marciniak, *Coord. Chem. Rev.*, 1990, **99**, 55–87.

16 W. A. Dar and K. Iftikhar, *Dalton Trans.*, 2016, **45**, 8956–8971.

17 R. Ilmi and K. Iftikhar, *Inorg. Chem. Commun.*, 2012, **20**, 7–12.

18 R. Ilmi, N. Hasan, J. Liu, D. Mara, R. Van Deun and K. Iftikhar, *J. Photochem. Photobiol., A*, 2017, **347**, 116–129.

19 C. R. De Silva, R. Wang and Z. Zheng, *Polyhedron*, 2006, **25**, 3449–3455.

20 R. Ilmi and K. Iftikhar, *J. Photochem. Photobiol., A*, 2017, **333**, 142–155.

21 R. Ilmi and K. Iftikhar, *Inorg. Chem. Commun.*, 2010, **13**, 1552–1557.

22 R. Ilmi and K. Iftikhar, *Polyhedron*, 2015, **102**, 16–26.

23 C.-Q. Shen, T.-L. Yan, Y.-T. Wang, Z.-J. Ye, C.-J. Xu and W.-J. Zhou, *J. Lumin.*, 2017, **184**, 48–54.

24 K. Binnemans, *Coord. Chem. Rev.*, 2015, **295**, 1–45.

25 G. F. de Sá, O. L. Malta, C. de Mello Donegá, A. M. Simas, R. L. Longo, P. A. Santa-Cruz and E. F. da Silva, *Coord. Chem. Rev.*, 2000, **196**, 165–195.

26 R. G. Charles and A. Perrotto, *J. Inorg. Nucl. Chem.*, 1964, **26**, 373–376.

27 E. Niyama, H. F. Brito, M. Cremona, E. E. S. Teotonio, R. Reyes, G. E. S. Brito and M. C. F. C. Felinto, *Spectrochim. Acta, Part A*, 2005, **61**, 2643–2649.

28 H. Brito, C. Carvalho, O. Malta, J. Passos, J. Menezes and R. Sinisterra, *Spectrochim. Acta, Part A*, 1999, **55**, 2403–2410.

29 T. Hou, J. Bian, X. Yue, S. Yue and J. Ma, *Inorg. Chim. Acta*, 2013, **394**, 15–20.

30 S. Yue, N. Li, J. Bian, T. Hou and J. Ma, *Synth. Met.*, 2012, **162**, 247–256.

31 W. A. Dar, A. B. Ganaie and K. Iftikhar, *J. Lumin.*, 2018, **202**, 438–449.

32 M. H. V. Werts, R. T. F. Jukes and J. W. Verhoeven, *Phys. Chem. Chem. Phys.*, 2002, **4**, 1542–1548.

33 M. I. Aroyo, International Tables for Crystallography, International Union of Crystallography, Chester, England, 2016.

34 K. Binnemans, K. Lodewyckx, T. N. Parac-Vogt, R. Van Deun, B. Goderis, B. Tinant, K. Van Hecke and L. Van Meervelt, *Eur. J. Inorg. Chem.*, 2003, 3028–3033.

35 F. H. Allen, *Acta Crystallogr., Sect. B: Struct. Sci.*, 2002, **58**, 380–388.

36 T. Tsukuda, T. Suzuki and S. Kaizaki, *Inorg. Chim. Acta*, 2005, **358**, 1253–1257.

37 X.-L. Mei, Y. Ma, L.-C. Li and D.-Z. Liao, *Dalton Trans.*, 2012, **41**, 505–511.

38 Y.-L. Wang, Y. Ma, X. Yang, J. Tang, P. Cheng, Q.-L. Wang, L.-C. Li and D.-Z. Liao, *Inorg. Chem.*, 2013, **52**, 7380–7386.

39 G. Stupka, L. Gremaud and A. F. Williams, *Helv. Chim. Acta*, 2005, **88**, 487–495.

40 M. J. Lacey, C. G. Macdonald and J. S. Shannon, *Org. Mass Spectrom*, 1968, **1**, 115–126.

41 A. P. Hunter, A. M. J. Lees and A. W. G. Platt, *Polyhedron*, 2007, **26**, 4865–4876.

42 Y. Hasegawa and T. Nakanishi, *RSC Adv.*, 2015, **5**, 338–353.

43 A. K. Singh, S. K. Singh, H. Mishra, R. Prakash and S. B. Rai, *J. Phys. Chem. B*, 2010, **114**, 13042–13051.

44 Y. Wang, Y.-L. Zhang, W. Dou, A. Zhang, W. Qin and W. Liu, *Dalton Trans.*, 2010, **39**, 9013.

45 S. V. Eliseeva, D. N. Pleshkov, K. A. Lyssenko, L. S. Lepnev, J.-C. G. Bünzli and N. P. Kuzmina, *Inorg. Chem.*, 2011, **50**, 5137–5144.

46 A. Josephine Kanimozhi and V. Alexander, *Dalton Trans.*, 2017, **46**, 8562–8571.

47 Z. A. Taha, A. M. Ajlouni, A. K. Hijazi, N. A. Al-Rawashdeh, K. A. Al-Hassan, Y. A. Al-Haj, M. A. Ebqa'ai and A. Y. Altalafha, *J. Lumin.*, 2015, **161**, 229–238.

48 L. F. Marques, H. P. Santos, K. A. D'Oliveira, N. P. Botezine, M. C. R. Freitas, R. O. Freire, J. D. L. Dutra, J. S. Martins, C. Legnani, W. G. Quirino and F. C. Machado, *Inorg. Chim. Acta*, 2017, **458**, 28–38.

49 H.-Y. Wong, W.-S. Lo, W. T. K. Chan and G.-L. Law, *Inorg. Chem.*, 2017, **56**, 5135–5140.

50 Z. Ahmed and K. Iftikhar, *Polyhedron*, 2015, **85**, 570–592.

51 Z. Ahmed and K. Iftikhar, *Inorg. Chem.*, 2015, **54**, 11209–11225.

52 M. Pietraszkiewicz, O. Pietraszkiewicz, J. Karpiuk, A. Majka, G. Dutkiewicz, T. Borowiak, A. M. Kaczmarek and R. Van Deun, *J. Lumin.*, 2016, **170**, 411–419.

53 F. Zhang, Y. Hou, C. Du and Y. Wu, *Dalton Trans.*, 2009, 7359.

54 N. S. Kariaka, V. A. Trush, S. S. Smola, Y. M. Fadieiev, V. V. Dyakonenko, S. V. Shishkina, T. Y. Sliva and V. M. Amirkhanov, *J. Lumin.*, 2018, **194**, 108–115.

55 D. M. Roitershtein, L. N. Puntus, K. A. Lyssenko, I. V. Taidakov, E. A. Varaksina, M. E. Minyaev, V. A. Gerasin, M. A. Guseva, A. A. Vinogradov, M. S. Savchenko and I. E. Nifant'ev, *New J. Chem.*, 2017, **41**, 13663–13672.

56 A. F. Kirby and F. S. Richardson, *J. Phys. Chem.*, 1983, **87**, 2544–2556.

57 G. Blasse, *Inorg. Chim. Acta*, 1988, **142**, 153–154.

58 A. S. Souza and M. A. Couto dos Santos, *Chem. Phys. Lett.*, 2012, **521**, 138–141.

59 H.-G. Liu, Y.-I. Lee, S. Park, K. Jang and S. S. Kim, *J. Lumin.*, 2004, **110**, 11–16.

60 L. Wang, X. Wang, T. Wang, Z. Hu, G. Zou and Q. Zhang, *J. Mater. Sci.*, 2012, **47**, 2600–2606.

61 Q.-F. Li, L. Jin, L. Li, W. Ma, Z. Wang and J. Hao, *J. Mater. Chem. C*, 2017, **5**, 4670–4676.

62 W.-S. Lo, J. Zhang, W.-T. Wong and G.-L. Law, *Inorg. Chem.*, 2015, **54**, 3725–3727.

63 J.-S. Kang, Y.-K. Jeong, Y. S. Shim, S. Rout, K. T. Leung, Y. Sohn and J.-G. Kang, *J. Lumin.*, 2016, **178**, 368–374.

64 K. Iftikhar, *Polyhedron*, 1996, **15**, 1113–1120.

65 K. Binnemans and C. Görller-Walrand, *Chem. Phys. Lett.*, 1995, **235**, 163–174.

66 W. A. Dar, Z. Ahmed and K. Iftikhar, *J. Photochem. Photobiol., A*, 2018, **356**, 502–511.

67 T. Kushida and M. Tanaka, *Phys. Rev. B: Condens. Matter Mater. Phys.*, 2002, **65**, 195118.